

# Thermotropic Liquid Crystals of a Non-Mesogenic Group Bearing Surfactant-Encapsulated Polyoxometalate Complexes

Xiankun Lin, Wen Li, Jing Zhang, Hang Sun, Yi Yan, and Lixin Wu\*

State Key Laboratory of Supramolecular Structure and Materials, Jilin University, Changchun 130012, People's Republic of China

Received May 14, 2010. Revised Manuscript Received June 28, 2010

A tri(ethylene oxide)octadecyldimethylammonium *p*-toluenesulfonate ( $C_{18}NEO_3 \cdot Ts$ ) amphiphile was employed to encapsulate Keggin-type polyoxometalates by ion metathesis reactions with phosphotungstic acid, silicotungstic acid, pentapotassium dodecatungstoborate(III), and phosphomolybdic acid, giving the surfactant-encapsulated polyoxometalates (SEPs) in SEP-P, SEP-Si, SEP-B, and SEP-PMo, respectively. Meanwhile, a  $C_{18}NEO_3 \cdot PF_6$  amphiphile was prepared by substituting the *p*-toluenesulfonate of  $C_{18}NEO_3 \cdot Ts$  with hexafluorophosphate. The chemical composition of all SEPs and amphiphiles was characterized through  $^1H$  NMR, infrared spectroscopy, mass spectroscopy, elemental analysis, and thermogravimetric analysis. The thermal properties of the SEPs and the amphiphiles were investigated by differential scanning calorimetry, polarized optical microscopy, and variable-temperature X-ray diffraction. The types of anions have a remarkable influence on the thermal properties of the prepared compounds or complexes.  $C_{18}NEO_3 \cdot Ts$  displays a smectic A phase with low transition temperatures, and  $C_{18}NEO_3 \cdot PF_6$  is a near-room-temperature ionic liquid. In contrast to the fact that SEP-Si and SEP-PMo decompose upon just reaching or before reaching the isotropic liquid state, both SEP-P and SEP-B reveal smectic B phase structures. The present results indicate that the combination of proper cationic amphiphiles and polyoxometalates can impart typical thermotropic liquid-crystalline behavior to SEPs, although no mesogenic groups are introduced into the complex systems.

## Introduction

Liquid crystals (LCs), as a fascinating class of supramolecular soft matter, have attracted considerable attention because of fundamental interest and potential applications. As a consequence of possessing fluidity like that of isotropic liquids and anisotropic structures like those of crystals, LCs are able to respond to external stimuli reversibly and exhibit functionalities such as anisotropic optical, electrical, and conductive properties, leading to various applications such as displays, ion-conductive materials, and sensors.<sup>1–7</sup> In recent years, one of the hot points in LC research is organic–inorganic hybrid liquid crystals, especially in the introduction of inorganic functional nanoobjects such as gold,<sup>8–10</sup> anisotropic  $TiO_2$ ,<sup>11</sup> and  $Fe_2O_3$  nanoparticles,<sup>12</sup> silsesquioxanes,<sup>13</sup> and inorganic clusters<sup>14,15</sup> into liquid crystals, owing to the diverse advantages provided by such a combination. On one

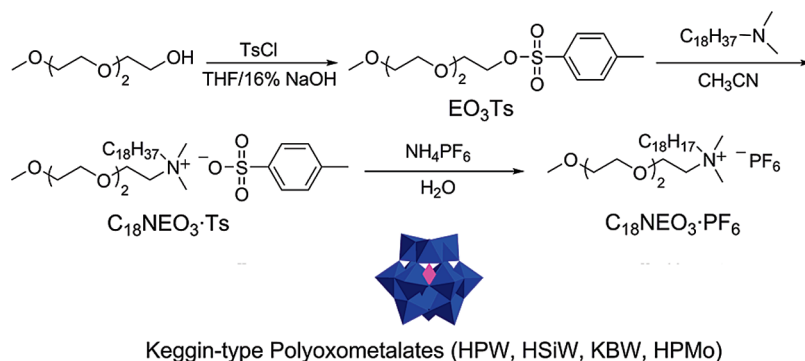
hand, LCs can afford an ordered microenvironment for the organization and arrangement of nanoobjects as well as the optimization of manifold properties.<sup>16</sup> On the other hand, the introduced nanoobjects can provide new properties to LCs through realizing the synergy with LCs toward functional soft materials.<sup>17</sup>

Among these numerous nanoobjects, a special one is metal oxides or polyoxometalates (PMs). As a kind of multiply charged nanoscale inorganic cluster, PMs possess structure and property advantages as well as promising applications in many areas including catalysis, optics, electronics, and magnetics and are considered to be fascinating building blocks for supramolecular architectures and functional hybrid materials.<sup>18–20</sup> Pioneering research results with the aim of incorporating PMs into thermotropic liquid crystals through the encapsulation of PMs with organic surfactants have been obtained in recent years. Among the designed surfactant-encapsulated PM (SEP) building blocks for LCs, modification of the surfactants with mesogenic groups such as azobenzene or biphenyl groups or precursors for hydrogen-bonding dimers was found to be necessary to endow the obtained SEPs with tunable thermotropic liquid-crystalline properties.<sup>21–25</sup>

\*To whom correspondence should be addressed. E-mail: wulx@jlu.edu.cn.

- (1) Saez, I. M.; Goodby, J. W. *J. Mater. Chem.* **2005**, *15*, 26–40.
- (2) Goodby, J. W.; Saez, I. M.; Cowling, S. J.; Görtz, V.; Draper, M.; Hall, A. W.; Sia, S.; Cosquer, G.; Lee, S. E.; Raynes, E. P. *Angew. Chem., Int. Ed.* **2008**, *47*, 2754–2787.
- (3) Kato, T.; Mizoshita, N.; Kishimoto, K. *Angew. Chem., Int. Ed.* **2006**, *45*, 38–68.
- (4) Kato, T. *Science* **2002**, *295*, 2414–2418.
- (5) Ikeda, T.; Mamiya, J. I.; Yu, Y. *Angew. Chem., Int. Ed.* **2007**, *46*, 506–528.
- (6) Tschierske, C. *Chem. Soc. Rev.* **2007**, *36*, 1930–1970.
- (7) Binnemans, K. *Chem. Rev.* **2005**, *105*, 4148–4204.
- (8) Kanayama, N.; Tsutsumi, O.; Kanazawa, A.; Ikeda, T. *Chem. Commun.* **2001**, 2640–2641.
- (9) Cseh, L.; Mehl, G. H. *J. Am. Chem. Soc.* **2006**, *128*, 13376–13377.
- (10) Wojcik, M.; Lewandowski, W.; Matraszek, J.; Mieczkowski, J.; Borysiuk, J.; Pocięcha, D.; Gorecka, E. *Angew. Chem., Int. Ed.* **2009**, *48*, 5167–5169.
- (11) Kanie, K.; Sugimoto, T. *J. Am. Chem. Soc.* **2003**, *125*, 10518–10519.
- (12) Kanie, K.; Muramatsu, A. *J. Am. Chem. Soc.* **2005**, *127*, 11578–11579.
- (13) Elsaßer, R.; Mehl, G. H.; Goodby, J. W.; Photinos, D. J. *Chem. Commun.* **2000**, 851–852.
- (14) Terazzi, E.; Bourgogne, C.; Welter, R.; Gallani, J.-L.; Guillon, D.; Rogez, G.; Donnio, B. *Angew. Chem., Int. Ed.* **2008**, *47*, 490–495.
- (15) Nieuwenhuyzen, M.; Seddon, K. R.; Teixidor, F.; Puga, A. V.; Viñas, C. *Inorg. Chem.* **2009**, *48*, 889–901.

- (16) Zeng, X.; Liu, F.; Fowler, A. G.; Ungar, G.; Cseh, L.; Mehl, G. H.; Macdonald, J. E. *Adv. Mater.* **2009**, *21*, 1746–1750.
- (17) Nishizawa, K.; Nagano, S.; Seki, T. *Chem. Mater.* **2009**, *21*, 2624–2631.
- (18) Special issue on polyoxometalates: *Chem. Rev.* **1998**, *98*, 1.
- (19) Pope, M. T.; Müller, A. *Angew. Chem., Int. Ed. Engl.* **1991**, *30*, 34–48.
- (20) Long, D.-L.; Burkholder, E.; Cronin, L. *Chem. Soc. Rev.* **2007**, *36*, 105–121.
- (21) Li, W.; Bu, W. F.; Li, H. L.; Wu, L. X.; Li, M. *Chem. Commun.* **2005**, 3785–3787.
- (22) Li, W.; Yin, S. Y.; Wu, Y. Q.; Wu, L. X. *J. Phys. Chem. B* **2006**, *110*, 16961–16966.
- (23) Yin, S. Y.; Li, W.; Wang, J. F.; Wu, L. X. *J. Phys. Chem. B* **2008**, *112*, 3983–3988.
- (24) Li, W.; Yin, S. Y.; Wang, J. F.; Wu, L. X. *Chem. Mater.* **2008**, *20*, 514–522.
- (25) Yin, S. Y.; Sun, H.; Yan, Y.; Li, W.; Wu, L. X. *J. Phys. Chem. B* **2009**, *113*, 2355–2364.

Scheme 1. Synthesis Route to  $C_{18}NEO_3 \cdot Ts$  and  $C_{18}NEO_3 \cdot PF_6$  and Polyhedron Structure of Keggin-Type PMs

A logic problem from a fundamental research point of view is whether SEPs exhibiting typical thermotropic liquid-crystalline behavior can be obtained through surfactants without mesogenic groups because, in some cases, aromatic mesogenic groups have intrinsic disadvantages. For example, they can disturb the specific properties of the inorganic clusters, such as the luminescence of PMs.<sup>25</sup> To obtain functional SEPs with thermotropic LC behavior, some efforts have been made by using simple surfactants without mesogenic groups to coordinate with the PMs, but the suggested LC behavior is often not typical and cannot be observed completely and clearly because of the decomposition of the complexes before reaching melting or clearing points.<sup>26–28</sup> Although surfactants without mesogenic groups have been used to assemble PMs into liquid-crystalline-like arrangements,<sup>28</sup> the SEPs possessing no mesogenic groups but exhibiting typical thermotropic LC properties have not yet, to the best of our knowledge, been reported.

Consequently, to endue SEPs with typical LC properties successfully requires the elaborate design of surfactants, the suitable selection of PMs, and the perfect combination. It is well known that the lengths of alkyl chains, the types of ions, and the types of heterocycles in ionic heads can affect the thermal properties of the ionic liquid crystals.<sup>29,30</sup> Here, we propose a new strategy to adjust the thermal properties of SEPs through regarding them as a class of special ionic complexes. Different from the common anions, PM polyanions possess a nanoscaled size, which provides large hydrophilic and ionic domains in the hydrophobic organized structures. Therefore, it is possible to alter the thermal properties of SEPs through introducing hydrophilic moieties (i.e., short poly(ethylene oxide) chains) into the ionic domains. Compared with the SEPs prepared using the simple surfactants, the introduction of hydrophilic moieties will increase the relative volume of hydrophilic domains in SEPs and could affect the packing efficiency of ions, which may result in depressed transition temperatures of SEPs. Moreover, SEPs could hold thermal stability when reaching the isotropic liquid state, which will make it possible for SEPs to show typical, reversible LC behavior without employing mesogenic groups.

In this study, we designed and synthesized amphiphilic diblock molecule  $C_{18}NEO_3 \cdot Ts$ , which bears a short tri(ethylene oxide)

(TEO) chain and a relatively long alkyl chain, as shown in Scheme 1. We expected that the TEO chain could serve as a hydrophilic moiety to affect the self-organized properties and thermal behavior of the obtained SEPs. The following results supported the proposed motivation and confirmed some new understanding of the PM-based LCs. Herein, we reported that certain SEPs, which do not contain mesogenic groups or precursors for hydrogen-bonding dimers, can maintain thermal stability when reaching the isotropic liquid state and exhibit typical thermotropic liquid crystals for the first time. We also found that introducing the TEO chains into SEPs is an efficient strategy for influencing the thermal properties of SEPs.

## Experimental Section

**Materials.** Unless otherwise noted, the chemicals were all obtained from commercial suppliers and used without further purification. Triethylene glycol monomethyl ether  $CH_3-(OCH_2CH_2)_3OH$  with a purity of 97% was purchased from Fluka, and *N,N*-dimethyloctadecylamine with a purity of 89% and ammonium hexafluorophosphate ( $NH_4PF_6$ ) with a purity of 99.5% were the product of Acros Organics. *p*-Toluenesulfonyl chloride (TsCl), phosphotungstic acid ( $H_3PW_{12}O_{40}$ , denoted as HPW), and silicotungstic acid ( $H_4SiW_{12}O_{40}$ , denoted as HSiW) were purchased from Sinopharm Chemical Reagent Co. Ltd. Phosphomolybdic acid ( $H_3PMo_{12}O_{40}$ , denoted as HPMo) was purchased from Alfa Aesar. Pentapotassium dodecatungstoborate(III) ( $K_5BW_{12}O_{40}$ , denoted as KBW) was synthesized according to a procedure in the literature.<sup>31</sup>

**Synthesis of Oligo(oxyethylene)octadecyldimethylammonium 4-Methylbenzenesulfonate ( $C_{18}NEO_3 \cdot Ts$ ).** The amphiphilic diblock molecule  $C_{18}NEO_3 \cdot Ts$  was synthesized according to a modified process.<sup>32</sup> Beginning with the tosylation of triethylene glycol monomethyl ether, the obtained product was allowed to react with *N,N*-dimethyloctadecylamine, giving the target product (Scheme 1).

To the mixture of  $CH_3(OCH_2CH_2)_3OH$  (8.24 g, 50.2 mmol) and 16% sodium hydroxide aqueous solution (17 mL) in an ice-salt bath was added dropwise the THF solution of TsCl (11.97 g, 62.8 mmol) with continuous stirring for 7 h. The resulting mixture was stirred at room temperature for another 27 h and then poured into ice water. The aqueous solution was extracted with three portions of chloroform. The combined organic extract was dried over anhydrous  $MgSO_4$ , filtered, and concentrated under reduced pressure to give product *p*-toluenesulfonyl tri(ethylene oxide) monomethyl ether ( $EO_3Ts$ ) (15.40 g) in a yield of 96.8% as a colorless liquid.  $^1H$  NMR (500 MHz,  $CDCl_3$ ,  $\delta$ ): 2.42 (s, 3H), 3.34 (s, 3H), 3.59–3.49 (m, 8H), 3.67 (t,  $J = 5$  Hz, 2H), 4.14 (t,  $J = 5$  Hz, 2H), 7.33 (d,  $J = 8$  Hz, 2H), 7.78 (d,  $J = 8$  Hz, 2H).

(31) Rocchiccioli-Deltcheff, C.; Fournier, M.; Franck, R.; Thouvenot, R. *Inorg. Chem.* **1983**, *22*, 207–216.

(32) Lin, X. K.; Wang, Y. L.; Wu, L. X. *Langmuir* **2009**, *25*, 6081–6087.

(26) Zhang, T. R.; Spitz, C.; Antonietti, M.; Faul, C. F. J. *Chem.—Eur. J.* **2005**, *11*, 1001–1009.

(27) Zhang, T. R.; Liu, S. Q.; Kurth, D. G.; Faul, C. F. J. *Adv. Funct. Mater.* **2009**, *19*, 642–652.

(28) Polarz, S.; Smarsly, B.; Antonietti, M. *ChemPhysChem* **2001**, *2*, 457–461.

(29) Goossens, K.; Lava, K.; Nockemann, P.; Hecke, K. V.; Meervelt, L. V.; Driesen, K.; Görlner-Walrand, C.; Binnemans, K.; Cardinaels, T. *Chem.—Eur. J.* **2009**, *15*, 656–674.

(30) Goossens, K.; Lava, K.; Nockemann, P.; Hecke, K. V.; Meervelt, L. V.; Pattison, P.; Binnemans, K.; Cardinaels, T. *Langmuir* **2009**, *25*, 5881–5897.

$\text{EO}_3\text{Ts}$  (6.52 g, 20.5 mmol) and *N,N*-dimethyloctadecylamine (6.86 g, 20.5 mmol) were dissolved in anhydrous acetonitrile. The mixture was refluxed for 27 h. Solvent was removed through evaporation, and the crude product was purified by silica gel column chromatography with chloroform/methanol (10:1 v/v) as the eluent to give the compound  $\text{C}_{18}\text{NEO}_3 \cdot \text{Ts}$  (3.80 g, 30.1%) as a white solid.  $^1\text{H}$  NMR (500 MHz,  $\text{CDCl}_3$ ,  $\delta$ ): 7.78 (d,  $J = 8$  Hz, 2H), 7.15 (d,  $J = 8$  Hz, 2H), 3.96 (t,  $J = 5$  Hz, 2H), 3.82 (t,  $J = 5$  Hz, 2H), 3.64–3.50 (m, 8H), 3.46 (m, 2H), 3.35 (s, 3H), 3.30 (s, 6H), 2.33 (s, 3H), 1.70 (m, 2H), 1.26 (m, 30H), 0.88 (t,  $J = 7$  Hz, 3H). IR (KBr): 3467, 3031, 2954, 2923, 2852, 1635, 1468, 1353, 1303, 1196, 1122, 1035, 1014, 816, 717, 681  $\text{cm}^{-1}$ . Matrix-assisted laser desorption/ionization time-of-flight mass spectrometry (MALDI-TOF MS) ( $m/z$ ): 444.4  $[\text{M} - \text{Ts}]^+$ , 171.0  $[\text{Ts}]^-$ .

**Synthesis of Oligo(oxyethylene)octadecyldimethylammonium Hexafluorophosphate ( $\text{C}_{18}\text{NEO}_3 \cdot \text{PF}_6$ ).** The diblock molecule  $\text{C}_{18}\text{NEO}_3 \cdot \text{PF}_6$  was prepared through a metathesis reaction in water; that is, the *p*-toluenesulfonate in  $\text{C}_{18}\text{NEO}_3 \cdot \text{Ts}$  was exchanged for hexafluorophosphate (Scheme 1).

$\text{C}_{18}\text{NEO}_3 \cdot \text{Ts}$  (0.28 g, 0.46 mmol) in water (5 mL) was stirred at room temperature, and then  $\text{NH}_4\text{PF}_6$  (0.39 g, 2.39 mmol) dissolved in water (10 mL) was added dropwise. A white precipitate formed immediately, and the reaction mixture was stirred for 30 min. The sticky precipitate was separated by pouring out the supernatant, and then the precipitate was dissolved in chloroform. The organic phase was washed with three portions of water, dried over anhydrous  $\text{MgSO}_4$ , filtered, and concentrated under reduced pressure to give the product as a white solid (0.23 g) in a yield of 85.4%.  $^1\text{H}$  NMR (500 MHz,  $\text{CDCl}_3$ ,  $\delta$ ): 3.93 (t, 2H), 3.68–3.51 (m, 10H), 3.36 (s, 3H), 3.34 (m, 2H), 3.14 (s, 6H), 1.72 (m, 2H), 1.26 (m, 30H), 0.88 (t,  $J = 7$  Hz, 3H). IR (KBr): 3426, 2953, 2919, 2851, 1623, 1471, 1355, 1299, 1252, 1200, 1122, 1029, 835, 721  $\text{cm}^{-1}$ . MALDI-TOF MS ( $m/z$ ): 444.4  $[\text{M} - \text{PF}_6]^+$ , 145.0  $[\text{PF}_6]^-$ . Anal. Calcd for  $\text{C}_{18}\text{NEO}_3 \cdot \text{PF}_6$  ( $\text{C}_{27}\text{H}_{58}\text{F}_6\text{NO}_3\text{P}$ , 589.72): C, 54.99; H, 9.91; N, 2.38. Found: C, 55.12; H, 9.89; N, 2.03.

**Preparation of SEPs.** The diblock molecule  $\text{C}_{18}\text{NEO}_3 \cdot \text{Ts}$  was employed to prepare complexes SEP-P, SEP-Si, SEP-B, and SEP-PMo through the metathesis reaction with HPW, HSiW, HBW, and HPMo, respectively. The preparation processes for all of the SEPs are similar. Taking the preparation of SEP-P as an example, its detailed procedure is as follows.

**SEP-P.**  $\text{C}_{18}\text{NEO}_3 \cdot \text{Ts}$  (0.15 g, 0.24 mmol) in water (6 mL) was stirred at room temperature, and then HPW (0.23 g, 0.08 mmol) dissolved in water (4 mL) was added dropwise. A white precipitate formed immediately and was collected by filtration and washed with a bit of water. The obtained crude product was purified further through recrystallization from chloroform/methanol, giving the complex as a white needlelike material (0.26 g) in a yield of 77.8%.  $^1\text{H}$  NMR (500 MHz,  $\text{CDCl}_3$ ,  $\delta$ ): 0.88 (t,  $J = 7$  Hz, 3H), 1.26 (m, 30H), 1.81 (m, 2H), 3.32 (s, 6H), 3.37 (s, 3H), 3.45 (m, 2H), 3.54–3.74 (m, 10H), 4.15 (m, 2H). IR (KBr): 2956, 2925, 2852, 1468, 1350, 1293, 1253, 1200, 1111, 1079, 977, 896, 811  $\text{cm}^{-1}$ . Anal. Calcd for SEP-P ( $\text{C}_8\text{H}_{174}\text{N}_3\text{O}_{49}\text{PW}_{12}$ , 4211.29): C, 23.10; H, 4.17; N, 1.00. Found: C, 22.99; H, 4.56; N, 0.73. SEP-P should correspond to the formula  $(\text{C}_{18}\text{NEO}_3)_3\text{PW}_{12}\text{O}_{40}$ .

**SEP-Si.** This compound complex was prepared by following a procedure similar to that for SEP-P by using HSiW instead. The initial molar ratio of  $\text{C}_{18}\text{NEO}_3 \cdot \text{Ts}$  to HSiW was controlled at 4:1. The complex was obtained as a white flake-like material (0.14 g) in a yield of 60.3%.  $^1\text{H}$  NMR (500 MHz,  $\text{CDCl}_3$ ,  $\delta$ ): 0.88 (t,  $J = 7$  Hz, 3H), 1.26 (m, 30H), 1.79 (m, 2H), 3.36 (s, 6H), 3.37 (s, 3H), 3.46 (m, 2H), 3.55–3.73 (m, 8H), 3.81 (m, 2H), 4.19 (m, 2H). IR (KBr): 3440, 2956, 2923, 2852, 1630, 1467, 1351, 1300, 1256, 1200, 1110, 1012, 973, 918, 884, 791  $\text{cm}^{-1}$ . Anal. Calcd for SEP-Si ( $\text{C}_{108}\text{H}_{232}\text{N}_4\text{O}_{52}\text{SiW}_{12}$ , 4653.16): C, 27.88; H, 5.03; N, 1.20. Found: C, 27.83; H, 5.04; N, 0.96. SEP-Si should correspond to the formula  $(\text{C}_{18}\text{NEO}_3)_4\text{SiW}_{12}\text{O}_{40}$ .

**SEP-B.** This compound complex was prepared by following a procedure similar to that for SEP-P by using KBW instead. The

initial molar ratio of  $\text{C}_{18}\text{NEO}_3 \cdot \text{Ts}$  to KBW was controlled at 5:1. The complex was obtained as a sticky white material (0.19 g) in a yield of 74.5%.  $^1\text{H}$  NMR (500 MHz,  $\text{CDCl}_3$ ,  $\delta$ ): 0.88 (t,  $J = 7$  Hz, 3H), 1.26 (m, 30H), 1.77 (m, 2H), 3.40 (s, 6H), 3.36 (s, 3H), 3.46 (m, 2H), 3.54–3.72 (m, 8H), 3.94 (m, 2H), 4.27 (m, 2H). IR (KBr): 3442, 2956, 2923, 2852, 1468, 1353, 1293, 1260, 1201, 1107, 951, 899, 816  $\text{cm}^{-1}$ . Anal. Calcd for SEP-B ( $\text{C}_{135}\text{H}_{290}\text{N}_5\text{O}_{55}\text{BW}_{12}$ , 5080.64): C, 31.91; H, 5.75; N, 1.38. Found: C, 32.41; H, 5.70; N, 1.15. SEP-B should correspond to the formula  $(\text{C}_{18}\text{NEO}_3)_5\text{BW}_{12}\text{O}_{40}$ .

**SEP-PMo.** This compound complex was prepared by following a procedure similar to that for SEP-P by using HPMo instead. The initial molar ratio of  $\text{C}_{18}\text{NEO}_3 \cdot \text{Ts}$  to HPMo was controlled at 3:1. The complex was obtained as a yellow needlelike material (0.15 g) in a yield of 67.8%.  $^1\text{H}$  NMR (500 MHz,  $\text{CDCl}_3$ ,  $\delta$ ): 0.88 (t,  $J = 7$  Hz, 3H), 1.26 (m, 30H), 1.82 (m, 2H), 3.34 (s, 6H), 3.38 (s, 3H), 3.46 (m, 2H), 3.55–3.73 (m, 10H), 4.13 (m, 2H). IR (KBr): 3427, 2956, 2923, 2852, 1467, 1352, 1296, 1261, 1199, 1107, 1062, 955, 879, 801  $\text{cm}^{-1}$ . Anal. Calcd for SEP-PMo ( $\text{C}_{81}\text{H}_{174}\text{N}_3\text{O}_{49}\text{PMo}_{12}$ , 3156.49): C, 30.82; H, 5.56; N, 1.33. Found: C, 30.56; H, 5.46; N, 1.16. SEP-PMo should correspond to the formula  $(\text{C}_{18}\text{NEO}_3)_3\text{PMo}_{12}\text{O}_{40}$ .

**Characterization.**  $^1\text{H}$  NMR spectra were recorded on a Bruker Avance 500 instrument using  $\text{CDCl}_3$  as the solvent and TMS as the internal reference. Infrared (IR) spectra were recorded on a Bruker Optics VERTEX 80v FT-IR spectrometer equipped with a DTGS detector (32 scans) with a resolution of 4  $\text{cm}^{-1}$  from pressed KBr pellets. Elemental analysis (C, H, N) was performed on a Vario EL elemental analyzer from Elementar Analysensysteme GmbH. Thermogravimetric analysis (TGA) was conducted with a PerkinElmer Diamond TG/DTA instrument with a heating rate of 10  $^\circ\text{C}/\text{min}$  under flowing air or  $\text{N}_2$ . MALDI-TOF MS spectra were recorded on an autoflex III smartbeam mass spectrometer (Bruker Daltonics Inc.) with  $\text{CHCl}_3$  as the solvent and dithranol (DIT) as the matrix or without a matrix. Polarized optical microscopy (POM) was performed using an Axioskop 40 polarized optical microscope (Carl Zeiss Light Microscopy, Germany) equipped with a LINKAM THMS 600 hot stage and a LINKAM CI 94 temperature controller. The pictures were captured through a ProgRes CT3 camera (JENOPTIK Laser, Optik, Systeme GmbH). Differential scanning calorimetry (DSC) measurements were performed on a Netzsch DSC 204 with scanning rate of 10  $^\circ\text{C}/\text{min}$ . The samples were sealed in aluminum capsules in air, and the atmosphere of the holder was sustained under dry nitrogen. For variable-temperature X-ray diffraction (XRD) experiments, a Bruker AXS D8 ADVANCE X-ray diffractometer using  $\text{Cu K}\alpha$  radiation with a wavelength of 1.5418  $\text{\AA}$  with an mri Physikalische Geräte GmbH TC-Basic temperature chamber was used. All samples were prepared by spreading the SEP solids on a thin, cleaned Si wafer, and the thermal history of the solids was eliminated before measurements.

## Results and Discussion

**Preparation of SEPs.** For the preparation of the SEPs, the  $\text{C}_{18}\text{NEO}_3 \cdot \text{Ts}$  amphiphile has been employed. The designed  $\text{C}_{18}\text{NEO}_3 \cdot \text{Ts}$  amphiphile is a substitute for octadecyltrimethylammonium *p*-toluenesulfonate, in which one of the methyl groups has been replaced by a tri(ethylene oxide) chain (Scheme 1). Because of the high solubility of  $\text{C}_{18}\text{NEO}_3 \cdot \text{Ts}$  in water, the common phase-transfer methods<sup>33</sup> are not applicable to encapsulating PMs, and the ion metathesis reaction in water was used in the present work. In addition, Keggin-type PMs, which possess pseudospherical structures, were chosen to prepare SEPs. In detail, HPW, HSiW, and KBW are polyoxotungstates with different central atoms, whereas HPMo possesses a structure that is

(33) Kurth, D. G.; Lehmann, P.; Volkmer, D.; Cölfen, H.; Koop, M. J.; Müller, A.; Chesne, A. D. *Chem.—Eur. J.* **2000**, *6*, 385–393.

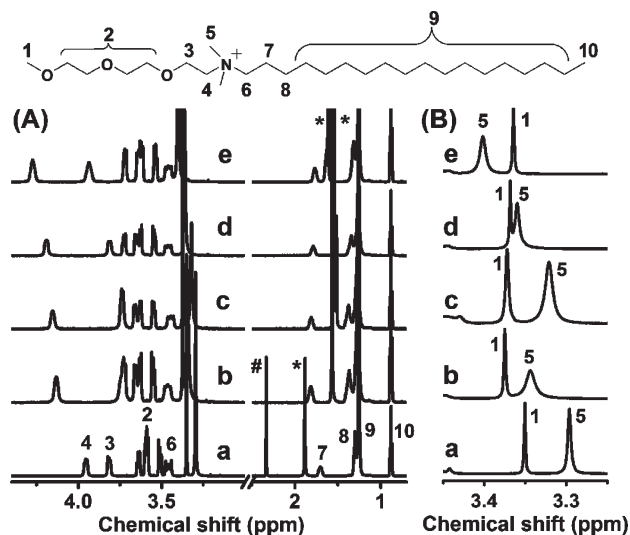


**Figure 1.**  $^1\text{H}$  NMR spectra of (a)  $\text{C}_{18}\text{NEO}_3\cdot\text{Ts}$ , (b) SEP-PMo, (c) SEP-P, (d) SEP-Si, and (e) SEP-B in the range of 0–5 ppm (A) and in the highlighted range of 3.25–3.45 ppm (B). The peak assignments have been marked with Arabic numbers. The peaks marked with stars correspond to the  $\text{H}_2\text{O}$  signal, and the symbol # represents the signal of the methyl group of *p*-toluenesulfonate.

similar to that of HPW except for different peripheral atoms. All of the employed PMs have the same volume. The four Keggin-type PMs, including HPW, HSiW, KBW, and HPMo, were complexed with  $\text{C}_{18}\text{NEO}_3\cdot\text{Ts}$  to give SEP-P, SEP-Si, SEP-B, and SEP-PMo as the precipitates, respectively. Direct precipitation from water usually provides the resulting electrostatic complexes with high-enough purity in the ionic assembly process.<sup>34</sup> However,  $^1\text{H}$  NMR spectra of unpurified precipitates indicate some compounds with *p*-toluenesulfonate, which may be derived from the adsorbed  $\text{C}_{18}\text{NEO}_3\cdot\text{Ts}$  remaining in the yielded precipitates. The impurity cannot be removed by washing. Fortunately, recrystallization from chloroform/methanol provides pure SEPs.

All of the SEPs were characterized through IR,  $^1\text{H}$  NMR, TGA, and elemental analysis, as shown in the Supporting Information and the Experimental Section. In the IR spectra of SEPs, the bands attributed to PMs remain but have obvious shifts, indicating that the structure of the PMs are maintained, and implying the interaction of cationic  $\text{C}_{18}\text{NEO}_3$  with PMs through electrostatic attraction.<sup>31</sup> Compared with the resonance signals of  $\text{C}_{18}\text{NEO}_3\cdot\text{Ts}$  alone,  $^1\text{H}$  NMR spectra of SEPs (Figure 1A,B) show the following points: (1) The peaks corresponding to *p*-toluenesulfonate totally disappear, indicating that organic cation  $\text{C}_{18}\text{NEO}_3$  is anchored firmly onto the polyanions and all of the SEPs are highly pure without the adsorbed  $\text{C}_{18}\text{NEO}_3\cdot\text{Ts}$  or *p*-toluenesulfonate acid or salts. (2) The chemical structure of cationic  $\text{C}_{18}\text{NEO}_3$  is also well maintained in the complexes. (3) The signals of the *N*-methyl proton in SEPs are shifted to low field. The signals in SEPs with the dioctadecyldimethylammonium cation are usually shifted to high field in contrast to that of surfactant dioctadecyldimethylammonium bromide.<sup>35</sup> The difference in the two situations originates from the different anions in the reference amphiphile (*p*-toluenesulfonate vs bromide). Different anions should have an influence on the electron cloud of the ammonium group. (4) Most signals that correspond to the TEO

**Table 1.** Summary of the Assignment of Mesophases, Phase-Transition Temperatures ( $^{\circ}\text{C}$ ), and Enthalpies (kJ/mol) of  $\text{C}_{18}\text{NEO}_3\cdot\text{Ts}$ ,  $\text{C}_{18}\text{NEO}_3\cdot\text{PF}_6$ , and All of the SEPs

	transition <sup>a</sup>	first cooling		second heating	
		$T$ ( $^{\circ}\text{C}$ )	$\Delta H$ (kJ/mol)	$T$ ( $^{\circ}\text{C}$ )	$\Delta H$ (kJ/mol)
$\text{C}_{18}\text{NEO}_3\cdot\text{Ts}$	S1–S2	–22.4	–1.3	–2.4	2.2
	S2–SmA	21.1	–42.9	35.6	39.3
	SmA–Iso	58.4	–0.7	60.9	0.7
$\text{C}_{18}\text{NEO}_3\cdot\text{PF}_6$	S1–S2	14.9	–14.3	20.3	14.7
	S2–Iso	37.9	–29.7	47.9	29.8
SEP-P	S1–S2	–16.2	–17.0	–11.0	25.5
	S2–SmB	181.4	–5.1	189.5	5.3
	SmB–Iso	214.9	–5.6	219.4	5.9
SEP-B	S–X	–12.9	–62.9	–6.3	63.0
	X–SmB	163.9	–3.4	200.9	2.7
	SmB–Iso	210.6	–2.8	216.7	3.5
SEP-Si	S1–S2	–33.9	–13.1	–30.8	12.5
	S2–S3 <sup>b</sup>	55.1	–12.5	72.0	12.5
SEP-PMo	S1–S2 <sup>c</sup>	–22.2	–17.6	–13.7	19.9

<sup>a</sup>S, SmA, SmB, Iso, and X indicate solid, smectic A, smectic B, isotropic liquid, and an unknown phase, respectively. <sup>b</sup>Decomposes when the sample reaches the isotropic liquid state. <sup>c</sup>Decomposes before melting.

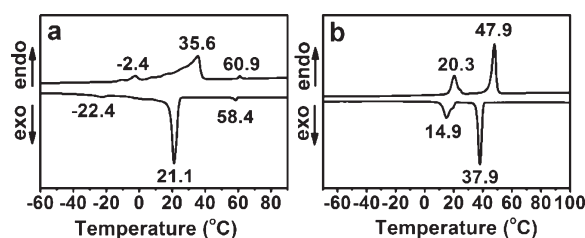


**Figure 2.** DSC curves of (a)  $\text{C}_{18}\text{NEO}_3\cdot\text{Ts}$  and (b)  $\text{C}_{18}\text{NEO}_3\cdot\text{PF}_6$  on their first cooling and second heating processes.

chains vary. Meanwhile, among the SEPs, these signals are also different. The variation confirms the influence of anions on TEO chains and implies that the TEO chains are close to the PMs although the organic cations are in a more free state in solution than in solid. In addition, the chemical shifts of most methyl or methylene protons near the nitrogen atom vary linearly as a function of the charge number of PMs in SEPs (Figure S10).

For all of the SEPs, no weight loss below  $150\text{ }^{\circ}\text{C}$  was observed according to the TGA curves (Figure S13). Thus, no crystalline water is considered in the resulting formulas of SEPs. According to elemental analysis, the formulas of SEPs are  $(\text{C}_{18}\text{NEO}_3)_3\text{-PW}_{12}\text{O}_{40}$  for SEP-P,  $(\text{C}_{18}\text{NEO}_3)_4\text{SiW}_{12}\text{O}_{40}$  for SEP-Si,  $(\text{C}_{18}\text{NEO}_3)_5\text{-BW}_{12}\text{O}_{40}$  for SEP-B, and  $(\text{C}_{18}\text{NEO}_3)_3\text{PMo}_{12}\text{O}_{40}$  for SEP-PMo. Here, the organic cations are denoted as  $\text{C}_{18}\text{NEO}_3$  for concise illustration. It should be noted that the protons in PMs have been totally exchanged in SEPs, which also implies that the interaction between the TEO chains and PMs bridged by oxonium ions is almost nonexistent in SEPs.<sup>32,36</sup>

**Thermal Properties of Amphiphiles.** The thermal properties of  $\text{C}_{18}\text{NEO}_3\cdot\text{Ts}$  and  $\text{C}_{18}\text{NEO}_3\cdot\text{PF}_6$  were investigated by DSC, POM, and XRD. Table 1 summarizes the phase-transition temperatures, enthalpies, and assignments of both amphiphiles.

According to the TGA results (Figure S12), both amphiphiles show very little weight loss below  $180\text{ }^{\circ}\text{C}$ , which is indicative of the thermal stability below that temperature. Figure 2a shows the DSC traces of  $\text{C}_{18}\text{NEO}_3\cdot\text{Ts}$  during its first cooling and second heating processes. During the first cooling process,  $\text{C}_{18}\text{NEO}_3\cdot\text{Ts}$  reveals three exothermic transitions at 58.4, 21.1, and  $-22.4\text{ }^{\circ}\text{C}$ . The enthalpy value for the phase transition at high temperature

(34) Faul, C. F. J.; Antonietti, M. *Chem.—Eur. J.* **2002**, *8*, 2764–2768.

(35) Bu, W. F.; Li, H. L.; Li, W.; Wu, L. X.; Zhai, C. X.; Wu, Y. Q. *J. Phys. Chem. B* **2004**, *108*, 12776–12782.

(36) Neumann, R.; Assael, I. J. *Chem. Soc., Chem. Commun.* **1989**, 547–548.

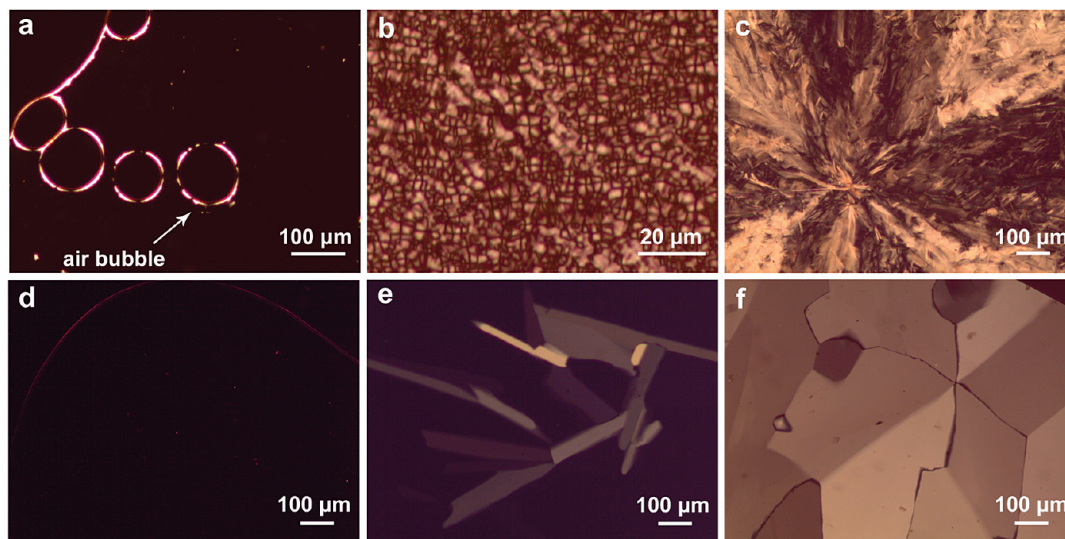


**Figure 3.** Polarized optical micrographs of  $C_{18}NEO_3 \cdot Ts$  at (a) 57 and (b) 54 °C, (c)  $C_{18}NEO_3 \cdot PF_6$  at 22 °C, SEP-P at (d) 222 and (e) 210 °C, and (f) SEP-B at 197 °C. Image d was captured during the first heating process, whereas the other images were captured during their first cooling runs.

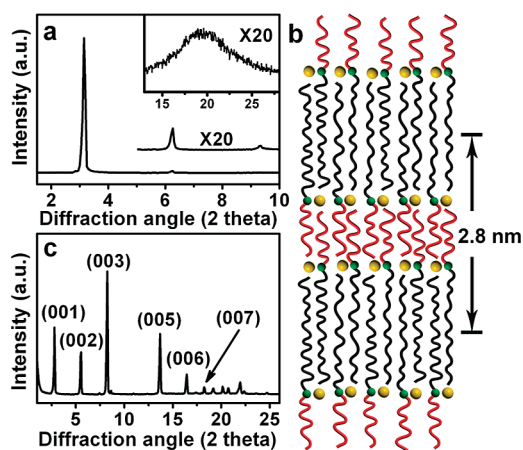


**Figure 4.** (a) XRD patterns of  $C_{18}NEO_3 \cdot Ts$  at 52 °C. (Inset) Corresponding magnification of the partial curve and a wide-angle XRD pattern. (b) Schematic model of the  $C_{18}NEO_3 \cdot Ts$  organized structure in the SmA phase. Black and red lines and green and yellow spheres represent alkyl and TEO chains and the quaternary ammonium headgroup and *p*-toluenesulfonate anion of  $C_{18}NEO_3 \cdot Ts$ , respectively. (c) XRD pattern of  $C_{18}NEO_3 \cdot PF_6$  at 30 °C.

(0.7 kJ/mol) is relatively small, obviously corresponding to the transition from an isotropic liquid to a less-ordered mesophase. The mesophase can be further assigned on the basis of its POM and XRD results. On cooling from the isotropic liquid state, the sample shows an all-black appearance (pseudo-isotropic texture) with some alignment-induced birefringent defects near air bubbles (Figure 3a). The focal conic texture appears only when a slight mechanical deformation was added by shearing the sample (Figure 3b). The XRD pattern of  $C_{18}NEO_3 \cdot Ts$  (Figure 4a) at 52 °C shows a sharp, intense diffraction peak with two weak subordinate diffraction peak in the small-angle region with *d*-spacings in a ratio of 1:1/2:1/3, suggesting a less-ordered layered structure with a layer spacing of 2.8 nm. In addition, a diffuse scattering halo at about *d* = 4.5 Å emerges in the wide-angle region, which is attributed to the disordered packing of alkyl chains. When the above results are combined, the phase between 58.4 and 21.1 °C could definitely be assigned as a smectic A (SmA)

phase. The phase transition at 21.1 °C shows a sharp exothermic peak and a large enthalpy (ca. −42.9 kJ/mol), suggesting a SmA–solid phase transition. In addition, the change at −22.4 °C is a solid–solid phase transition.

On the basis of the XRD results, a possible aggregation structure is assumed in the SmA phase, where the alkyl and TEO chains of individual  $C_{18}NEO_3 \cdot Ts$  compound are distributed at the opposite sides of the quaternary ammonium group because of microphase segregation. As a result of the quaternary ammonium group interacting with *p*-toluenesulfonate through electrostatic interaction, the cationic  $C_{18}NEO_3$  should penetrate and be normal to the ionic sublayer consisting of *p*-toluenesulfonate anions. Because the measured layer spacing is smaller than the ideal molecular length of  $C_{18}NEO_3$  with an all *trans* conformation of about 3.5 nm as calculated by the MM2 force field method, the conformation distortion can be imagined. Triethylene glycol monomethyl ether has a melting point below room temperatures. Therefore, in the SmA phase, TEO chains should adopt a contracted configuration,<sup>37</sup> which makes the interlayer distance smaller than the calculated length of  $C_{18}NEO_3$ . In addition, an increase of the gauche conformation of the alkyl chains is another reason for the short interlayer distance.<sup>22,24</sup> Thus, a double-layer structure can be expected in which the alkyl and TEO chains are fully interdigitated respectively, as illustrated in Figure 4b. It should be noted that the contraction of TEO chains on heating could also enlarge the lateral area of every alkyl chain, which leads to a low packing efficiency of ions in  $C_{18}NEO_3 \cdot Ts$ , and as a result, relatively low transition temperatures were found. Therefore,  $C_{18}NEO_3 \cdot Ts$  represents a new ionic liquid crystal, which exhibits a near-room-temperature melting point (35.6 °C) and a low clearing point.

In contrast to  $C_{18}NEO_3 \cdot Ts$ , the amphiphile  $C_{18}NEO_3 \cdot PF_6$ , which is the product in which the anion of  $C_{18}NEO_3 \cdot Ts$  is replaced by hexafluorophosphate, shows no LC properties. As shown by the DSC results (Figure 2b), the sharp endothermic peak and the large enthalpy (ca. 29.8 kJ/mol) at 47.9 °C suggest the melting of the  $C_{18}NEO_3 \cdot PF_6$  solid, which is further proven by POM and XRD results. When an isotropic liquid is cooled, the sample quickly forms spherulites with typical Maltese cross

(37) Kim, J.-U.; Lee, J.-C. *Macromol. Chem. Phys.* **2005**, *206*, 951–960.

extinction patterns (Figure 3c). The diameters of spherulites can reach several millimeters. Spherulites are often found in polymer systems, however, they can also appear in small molecules.<sup>38</sup> The XRD curve of  $C_{18}NEO_3 \cdot PF_6$  (Figure 4c) exhibits a crystalline layered structure with a layer spacing of 3.2 nm, as shown by several sharp equidistant diffraction peaks in the small-angle region at 30 °C. The irregular variation of the intensity of these diffraction peaks originates from the specific arrangement of the layers in the spherulites.<sup>39</sup> In the wide-angle region, several sharp diffraction peaks can be found, suggesting the highly ordered packing of the alkyl and TEO chains of  $C_{18}NEO_3$ . Evidently, the longer layer distance of  $C_{18}NEO_3 \cdot PF_6$  implies a more ordered packing of alkyl and TEO chains than that of  $C_{18}NEO_3 \cdot Ts$  in the SmA phase. Thus, the phase transitions at 47.9 and 20.3 °C can be assigned to the melting point and the solid–solid phase transition, respectively.

Normally, the microphase segregation of incompatible parts and the aggregation of compatible parts afford well-defined structures, the melting of long alkyl chains endows the mesophases with fluidity, and the electrostatic interaction stabilizes the layer structures and the interlayer bonding in the amphiphilic ionic liquid crystals, exhibiting smectic phases.<sup>40</sup> Moreover, weak electrostatic interaction is unfavorable to holding the positional order of mesophases. The electrostatic interaction between  $C_{18}NEO_3$  and the anion in  $C_{18}NEO_3 \cdot PF_6$  should be weaker than that in  $C_{18}NEO_3 \cdot Ts$ , similar to the situations in other ionic systems.<sup>41</sup> The electrostatic interaction in  $C_{18}NEO_3 \cdot PF_6$  seems too weak to keep the layered structures and endow  $C_{18}NEO_3 \cdot PF_6$  with LC behavior on heating, unlike the situation in  $C_{18}NEO_3 \cdot Ts$ . The weaker electrostatic forces of  $C_{18}NEO_3 \cdot PF_6$  should also lead to its lower transition temperature to an isotropic liquid compared to that of  $C_{18}NEO_3 \cdot Ts$ , although  $C_{18}NEO_3 \cdot PF_6$  forms highly ordered layered structures at near room temperature. Here, through a simple ion exchange, although  $C_{18}NEO_3 \cdot PF_6$  loses its LC properties, it reveals a new near-room-temperature ionic liquid.

**Thermal Properties of SEPs.** Both SEP-P and SEP-B show typical thermotropic liquid-crystalline properties and belong to enantiotropic LCs. Upon the first cooling, the DSC trace of SEP-P exhibits three exothermic transitions at 214.9, 181.4, and  $-16.2$  °C, respectively (Figure 5a). As shown in Table 1, the corresponding enthalpy values for the first two phase transitions are 5.6 and 5.1 kJ/mol, respectively. This trace is also similar to the DSC trace on the second heating, except for regular supercooling. SEP-B also exhibits three exothermic transitions appearing at 210.6, 163.9, and  $-12.9$  °C, respectively (Figure 5b). The enthalpy values for the first two phase transitions are 2.8 and 3.4 kJ/mol, respectively. It should be noted that the phase transition at 163.9 °C on the first cooling shows strong supercooling (about 37 °C) as well as a long transition as indicated by the relatively broad peak, compared with other transitions of SEP-B or SEP-P at high temperatures. This phenomenon should originate from the high viscosity of SEP-B, even at high temperatures.<sup>42</sup> Table 1 summarizes the phase-transition temperatures, enthalpies, and assignments of all of the SEPs. The calculated enthalpies of SEPs are attributed to the per molar SEP complex rather than the per molar organic cation. According to the TGA curves, the onset

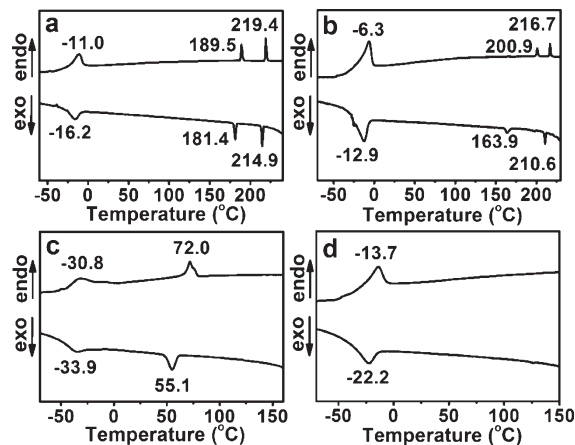


**Figure 5.** DSC curves of (a) SEP-P, (b) SEP-B, (c) SEP-Si, and (d) SEP-PMo on their first cooling and second heating processes.

temperatures of decomposition of SEP-P and SEP-B are 309 and 247 °C, respectively. The FT-IR spectra of SEP-P and SEP-B solids (Figure S14) that have been heated over clearing points are consistent with those without heat treatment, indicating that both SEPs are thermally stable when reaching the isotropic liquid state. In addition, all of the SEPs possess a higher thermal stability than  $C_{18}NEO_3 \cdot Ts$  and  $C_{18}NEO_3 \cdot PF_6$ , which is indicative of the dependence of the thermal stability on the anion type.<sup>30</sup>

The mesophases of SEP-P and SEP-B were further investigated by POM. The SEP-P sample becomes an isotropic liquid when it is heated to over ca. 220 °C (Figure 3d). In the following cooling run, SEP-P exhibits fluidity under shearing and a mosaic texture at 210 °C (Figure 3e). A mosaic texture is common for ordered smectic phases (i.e., the smectic B (SmB) phase), especially when a direct transition from an isotropic liquid occurs.<sup>43</sup> Meanwhile, large homeotropic domains are also observed, suggesting an orthogonal, optically uniaxial mesophase. For SEP-B, a typical mosaic texture was observed at 197 °C (Figure 3f) upon cooling from the isotropic liquid state (Figure S15). The high viscosity also makes the fluidity under shearing not obvious. However, the organized structure of SEP-B at the mesophase is mobile, and the appearance under POM observation rapidly changes from a mosaic texture to a pseudo-isotropic texture by shearing or decreasing temperature.

To identify the LC phases, we examined the possible packing structures of SEP-P and SEP-B. Figure 6a shows the variable-temperature XRD patterns of SEP-P. The reflection peaks corresponding to  $d$ -spacings of 2.6 and 1.3 nm in the small-angle region at 210 °C can be indexed as (001) and (002) for a layered structure with a layer spacing of 2.6 nm. Meanwhile, a single, moderately strong diffraction peak appears at  $2\theta \approx 21^\circ$ , indicating that a SmB phase exists.<sup>44</sup> Thus, the mesophase can be definitely assigned as a SmB phase. SEP-P shows a layered structure with a layer spacing of 2.7 nm at 30 °C. However, more than one diffraction peak exists in the wide-angle region, suggesting a more ordered structure. Thus, the phase-transition sequence of SEP-P can be concluded to be an Iso–SmB–solid2–solid1 process. Like SEP-P, SEP-B shows layered structures with layer spacings of 2.9 and 3.0 nm at 30 and 200 °C, respectively (Figure 6b). At 200 °C, a single diffraction peak appears at  $2\theta \approx 21^\circ$  in the wide-angle region, indicating that the mesophase is a

(38) Magill, J. H. *J. Mater. Sci.* **2001**, *36*, 3143–3164.

(39) Tanakaa, T.; Fujitaa, M.; Takeuchib, A.; Suzukib, Y.; Uesugib, K.; Doia, Y.; Iwata, T. *Polymer* **2005**, *46*, 5673–5679.

(40) Kanazawa, A.; Ikeda, T.; Nagase, Y. *Chem. Mater.* **2000**, *12*, 3776–3782.

(41) Bini, R.; Bortolini, O.; Chiappe, C.; Pieraccini, D.; Siciliano, T. *J. Phys. Chem. B* **2006**, *111*, 598–604.

(42) Wicklein, A.; Lang, A.; Muth, M.; Thelakkat, M. *J. Am. Chem. Soc.* **2009**, *131*, 14442–14453.

(43) Dierking, I. *Textures of Liquid Crystals*; Wiley-VCH: Weinheim, Germany, 2003.

(44) Demus, D.; Goodby, J. W.; Gray, G. W.; Spiess, H.-W.; Vill, V. *Handbook of Liquid Crystals*; Wiley-VCH: Weinheim, Germany, 1998; Vol. 1.

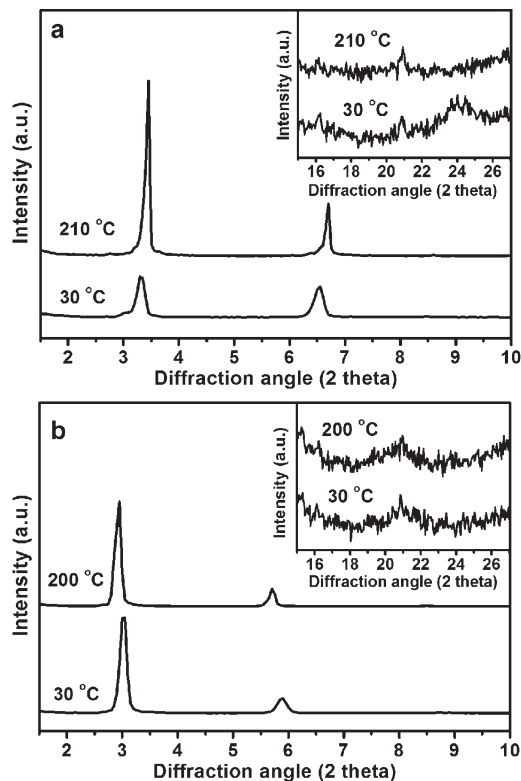
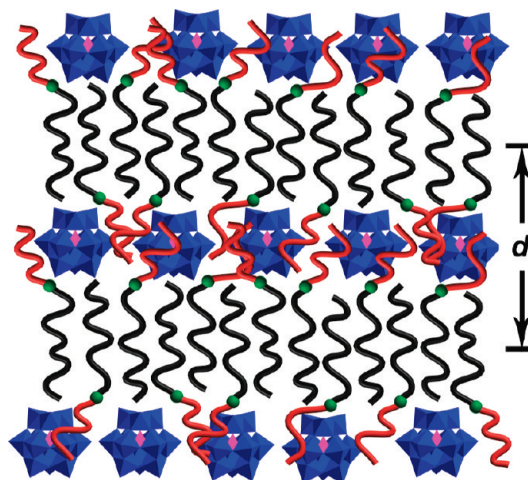


**Figure 6.** XRD patterns of (a) SEP-P and (b) SEP-B. (Inset) Corresponding wide-angle XRD patterns.

SmB phase. The diffraction patterns at both 30 and 200 °C are similar in the wide-angle region. However, the phase at 30 °C cannot be definitely assigned as an LC phase because typical textures and fluidity cannot be observed because of the high viscosity. This phase might not be in a crystalline state but may be in a highly ordered aggregated state.<sup>21</sup> Thus, the phase-transition sequence of SEP-B can be concluded to be an Iso–SmB–X–solid process.

On the basis of the above results, we tried to assume the packing structures of the SmB phases. Because of the incompatibility between the hydrophobic alkyl chain and the hydrophilic TEO chain in the cationic  $C_{18}NEO_3$ , the two tail chains are located on opposite sides of the quaternary ammonium group through microphase segregation. The TEO chains of  $C_{18}NEO_3$  are close to the PMs in the SEPs because both TEO chains and PMs are hydrophilic and the TEO chains are anchored onto PMs by the quaternary ammonium groups through electrostatic interactions. The  $^1H$  NMR result also indicates that the TEO chains and PMs are adjacent, as shown in Figure 1. Thus, hydrophobic domains consisting of alkyl chains and hydrophilic domains consisting of PMs and TEO chains will be generated, with the interface of the quaternary ammonium groups interacting with PMs. In addition, the length of the TEO chain with a fully extended conformation is about 1.2 nm, which is similar to the diameter ( $L_{PM}$ ) of the Keggin-type polyanion (1.0 nm).<sup>31,45</sup> Therefore, the contribution of TEO chains to the thickness of hydrophilic domains is faint and the thickness can be considered to be 1.0 nm, consistent with the size of PMs. The calculated length of the alkyl chain ( $L_A$ ) is about 2.3 nm. The layer spacings ( $d$ ) of both SEP-P (2.6 nm) and SEP-B (3.0 nm) in the SmB phase are smaller than the sum of  $L_A$  and  $L_{PM}$ . Thus, even if the alkyl

**Scheme 2. Schematic Illustration of Organized Structures in Mesophases of SEP-P or SEP-B<sup>a</sup>**



<sup>a</sup> The PMs are represented as blue polyhedrons. The alkyl and TEO chains and quaternary ammonium headgroup of  $C_{18}NEO_3$  are represented as black and red lines and green spheres, respectively.  $d$  is the layer spacing.

chains are fully interdigitated, the layer spacings are still smaller than the calculated one. This situation should originate from the contraction of the alkyl chains. In contrast to the situation in which PMs comprise hydrophilic domains by themselves, the additional TEO chains expand the lateral area of hydrophilic domains. As a result, the alkyl chains have to adopt a highly folded conformation to fill space effectively, which shortens the layer spacings. The highly folded alkyl chains also appear in some ionic liquid crystals.<sup>30</sup> Another possible reason may be the entrance of the quaternary ammonium groups of the surfactants into the PM sublayer, considering the pseudospherical structures of PMs. The reported crystalline structure of  $[SiM_{10}O_{40}][C_{16}H_{33}N(CH_3)_3]_4$  has shown that cetyltrimethylammonium cations can enter the PM sublayer.<sup>46</sup> Thus, we can propose a model for the packing structures of SEP-P and SEP-B in the SmB phases, as shown in Scheme 2. The hydrophilic sublayer containing TEO chains and polyanions is sandwiched by two uniform layers consisting of fully interdigitated alkyl chains. Alkyl chains with a highly folded conformation are perpendicular to the hydrophilic sublayer and possess bond orientational order. SEP-P, which possesses a lower alkyl chain density than that in SEP-B, has much more contracted alkyl chains than does SEP-B. Thus, the layer spacing of SEP-P in the SmB phase is visibly smaller than that of SEP-B.

Although SEP-P and SEP-B do not contain mesogenic groups, they possess amphiphilic structures that are similar to those of most ionic liquid crystals including  $C_{18}NEO_3 \cdot Ts$ , except for the PM anions that possess large volumes and numerous charges. Thus, the microphase segregation of incompatible parts and the aggregation of compatible parts are still the main driving forces for well-defined structures, and the long alkyl chains become necessary for microphase segregation and the fluidity of LC phases. When the anions are changed from *p*-toluenesulfonate in  $C_{18}NEO_3 \cdot Ts$  to PMs in SEPs, the electrostatic interaction between the anions and  $C_{18}NEO_3$  becomes stronger. As a result, the clearing points of SEP-P and SEP-B are higher than that of

(45) Bu, W. F.; Wu, L. X.; Zhang, X.; Tang, A. C. *J. Phys. Chem. B* **2003**, *107*, 13425–13431.

(46) Nyman, M.; Ingersoll, D.; Singh, S.; Bonhomme, F.; Alam, T. M.; Brinker, C. J.; Rodriguez, M. A. *Chem. Mater.* **2005**, *17*, 2885–2895.

$C_{18}NEO_3 \cdot Ts$ . Meanwhile, the electrostatic interactions in SEPs should be strong enough to stabilize the LC phases.

The present results are also consistent with the situation for the SEPs in which the surfactants with double tail chains are grafted with mesogenic groups (azobenzene or biphenyl groups).<sup>23,24</sup> In those cases, the match between the diameter of the PM and the cross-sectional diameter of the surfactant is regarded as an important factor that can determine the mesophases of the SEPs. When the occupied space of the individual surfactant on the surface of PM is large enough (i.e., HPW with only three charges was employed or HSiW polyanions were encapsulated by unprotonated surfactants), SmB phases can be observed.<sup>23,24</sup> However, when the surface of PM becomes crowded, SEPs have a SmA or smectic C phase if the charge number of polyanions increases<sup>24</sup> or if the surfactants are protonated for the SEP containing HSiW polyanions.<sup>23</sup> In contrast, cationic  $C_{18}NEO_3$  in SEP-P or SEP-B possesses only one alkyl chain. Therefore, the alkyl chains on the surfaces of PMs are not excessively crowded. Because of the synergy and matching between  $C_{18}NEO_3$  and the polyanions, an ordered smectic phase such as the SmB phase should be favorable to SEP-P. Obeying the same principle, SEP-B exhibits a SmB phase as well, whereas SEP, in which the KBW anions are encapsulated by the surfactants with double-tail chains, has SmA and smectic C phases.<sup>24</sup> The previous results have shown the situation in which the alkyl chains are too crowded to form the SmB phase,<sup>23,24</sup> whereas the present results indicate that the SmB phase can also form for SEP-P and SEP-B through the synergy and matching of organic and inorganic components, although only three alkyl chains per PM exist in SEP-P.

Unlike SEP-P and SEP-B, SEP-Si and SEP-PMo do not show typical LC behavior because no isotropic liquid state with thermal stability can be observed. Figure 5 shows the measured DSC traces of SEP-Si and SEP-PMo. Combined with the POM observation, SEP-Si reveals two solid–solid transitions at  $-30.8$  and  $72.0$  °C and SEP-PMo possesses only a solid–solid transition at  $-13.7$  °C on the second heating. Moreover, SEP-Si obviously decomposes while it reaches the isotropic liquid state (at ca.  $310$  °C as measured by POM), and SEP-PMo decomposes completely at ca.  $277$  °C before melting. These decompositions are in agreement with the corresponding TGA results.

#### **Influence of PMs on the Thermal Properties of SEPs.**

Comparing the four SEPs, they clearly show remarkable differences in thermal properties. Finally, we would like to determine the reason for this situation and the role of TEO chains. The prerequisite for obtaining SEPs that exhibit typical thermotropic LC properties is that the SEPs must maintain thermal stability when becoming isotropic liquids. Except for improving the thermal stability of the SEPs, adjusting the transition temperatures should be another effective means to access SEPs showing typical LC behavior. Although the electrostatic interaction still exists in the isotropic liquid state, ordered structures including the ionic sublayers should be effectively destroyed in ionic compounds.<sup>7</sup> Moreover, enhancing the interaction forces among the components or forming highly ordered structures can increase the transition temperatures to isotropic liquids.<sup>47</sup> The complex of  $C_{18}NEO_3$  with different PMs affords the resulting SEPs with different electrostatic interaction strength and different ion packing efficiencies and then varies the transition temperatures of SEPs. As shown in Figures 1 and S10, the signals of the *N*-methyl groups shift to low field with the increase in the charge number of PMs in

SEP-P, SEP-Si, and SEP-B. Considering that the PMs in SEPs have the same size, increasing the charge numbers will increase the charge density on the PMs and then enhance the electrostatic interaction between  $C_{18}NEO_3$  and PMs. Thus, the shifting scale of the *N*-methyl group signal can be regarded as an indicator of the strength of electrostatic interaction in SEPs, and the sequence of the electrostatic interaction strength is SEP-P < SEP-PMo < SEP-Si < SEP-B. In addition, the XRD patterns of the casting films of SEP-Si (Figure S16) show equidistant diffraction peaks in the small-angle region and several sharp diffraction peaks in the wide-angle region at  $30$  °C, implying that SEP-Si is prone to forming highly ordered layered structures. The SEP with the 1:4 cluster-to-surfactant ratio has been reported as a special situation in which single crystals can be obtained.<sup>46</sup> Here, SEP-Si should adopt a similar high packing efficiency of ions. However, compared with SEP-Si, the other three SEPs should possess lower packing efficiencies and have noncompact or crowded packing of alkyl chains because of more or fewer organic cations in these SEPs than in SEP-Si. Besides, all of the SEPs possess phase transitions with relatively large enthalpies below  $0$  °C (Figure 5), which are difficult to assign precisely. We thought that these transitions may be attributed to the phase transitions of alkyl chains.<sup>37</sup> The variation of enthalpies at these phase transitions among SEPs may also originate from the different packing efficiencies of ions in SEPs. Moreover, SEP-Si shows different thermal properties than other SEPs; that is, only SEP-Si has phase transitions between  $0$  and  $150$  °C, which may be relative to its unique, highly ordered packing structures.

By combining the above situations, we can give a plausible explanation for the dramatic difference in the thermal properties of SEPs when varying only the employed PMs. SEP-P possesses a lower packing efficiency than SEP-Si, that is, noncompact packing. Meanwhile, the electrostatic interaction in SEP-P is weakest among those of the present SEPs. These factors contribute to the relatively low clearing point of SEP-P. SEP-PMo contains the same quantity of cations as SEP-P, which should result in a similar packing efficiency to that of SEP-P. However, SEP-PMo has stronger electrostatic forces than does SEP-P, which should originate from the variation of peripheral atoms in PMs from W to Mo and the corresponding change in the charge distribution on the surfaces of PMs. Thus, SEP-PMo should possess a higher transition temperature than that of SEP-P so that it decomposes before melting. SEP-Si has stronger electrostatic forces than the two former SEPs and the highest packing efficiency among the present SEPs, which results in a transition temperature to an isotropic liquid state that is higher than the transition temperature of SEP-P. Considering the thermal stability, SEP-Si unfortunately decomposes when reaching the isotropic liquid state. Although SEP-B has the strongest electrostatic interactions, it may possess the lowest packing efficiency of ions among the four SEPs. The effect of low packing efficiency on the clearing point should surpass that of strong electrostatic interactions in SEP-B. Thus, SEP-B also has a relatively low clearing point and its LC behavior can be investigated clearly. Meanwhile, the clearing point and the corresponding entropy of SEP-B are a bit smaller than that of SEP-P. The low packing efficiency should also make SEP-B unable to form regular morphologies by recrystallization from the mixed organic solvent, unlike other SEPs.

It is worth noting that grafting TEO chains onto common cationic surfactants offers greater opportunity than using only the simple surfactants to adjust the packing efficiency of ions and the thermal properties of SEPs. The additional TEO chains can enter the hydrophilic domains containing PMs and could influence the thermal properties of SEPs. In contrast to the hydrophilic

(47) Wasserscheid, P.; Welton, T. *Ionic Liquids in Synthesis*; Wiley-VCH: Weinheim, Germany, 2002; Chapter 3.

domains that contain only polyanions, the TEO chains can make the hydrophilic domains more sensitive to heat, which promotes the collapse of the hydrophilic domains on heating. The TEO chains can also increase the volume of the hydrophilic parts in SEPs and adjust the packing efficiency of all components in SEPs, especially the packing and conformation of alkyl chains. Therefore, introducing TEO chains contributes to the decrease in the transition temperatures to the isotropic liquid state and endowing SEP-P and SEP-B with typical thermotropic LC behavior. Although the  $C_{18}NEO_3$  cation is not universal for affording the SEPs with LC properties among all of the PMs, the present method provides a good opportunity to access SEPs showing typical thermotropic LC behavior without containing mesogenic groups.

### Conclusions

Without the introduction of mesogenic groups or hydrogen bonding precursors, we have obtained SEPs that exhibit typical thermotropic LC properties through encapsulating HPW or KBW polyanions by using  $C_{18}NEO_3$ . The microphase segregation of incompatible parts and the aggregation of compatible parts, the long alkyl chains, and the electrostatic interactions with enough strength are key conditions for endowing  $C_{18}NEO_3 \cdot Ts$ , SEP-P, and SEP-B with typical LC behavior.  $C_{18}NEO_3 \cdot Ts$  shows a SmA phase with low transition temperatures, and SEP-P and SEP-B show typical SmB phases, whereas  $C_{18}NEO_3 \cdot PF_6$  is

a near-room-temperature ionic liquid. Adjusting the packing efficiency of the ions through introducing the TEO chains into SEPs is an efficient way to influence the thermal properties of SEPs, especially the transition temperatures to the isotropic liquid state, although SEP-Si and SEP-PMo do not show typical LC behavior. The present results indicate that the combination of proper cationic amphiphiles and PMs can impart typical thermotropic LC behavior to the obtained SEPs, and mesogenic groups or hydrogen bonding precursors are not necessary. We believe that the present method could facilitate the preparation and application of PM-based LC materials and might be feasible for other hybrid LCs based on nanoobjects.

**Acknowledgment.** This work was financially supported by the National Basic Research Program (2007CB808003), the National Natural Science Foundation of China (20973082, 20703019, 20921003), and the Open Project of State Key Laboratory of Polymer Physics and Chemistry, CAS. We thank the 111 project (B06009) for the visit and helpful discussions with Prof. Ulrich Körtz at Jacobs University.

**Supporting Information Available:** Characterization of  $C_{18}NEO_3 \cdot Ts$ ,  $C_{18}NEO_3 \cdot PF_6$ , and SEPs and XRD patterns of the casting films of SEP-Si. This material is available free of charge via the Internet at <http://pubs.acs.org>.